Heat Input and Gas Protection Influence on Welding Metallurgy of Cobalt Stainless Steel Coatings

Anderson Geraldo Marenda Pukasiewicz, anderson @utfpr.edu.br
Aldo Braghini Júnior, aldo@utfpr.edu.br
Rodrigo de Geus Kruppa, rodrigokruppa@yahoo.com.br
UTFPR universidade Tecnológica Federal do Paraná - Campus Ponta Grossa, Av. Monteiro Lobato s/n, km04, Ponta Grossa, Paraná, Brasil, CEP 84016-210

André Ricardo Capra, andre.capra@lactec.org.br
LACTEC, Instituto de Tecnologia para o Desenvolvimento, Curitiba, Paraná, Brasil,
Av. Lothário Meissner, nº01, Jardim Botânico, Curitiba, Paraná, Brasil, CEP 80210-170

Abstract. *ASTM A743-CA6NM stainless steel has adequate cavitation and corrosion resistance with good weldability, because of these properties it have been used in hydraulic turbine runners. However this class of steel have some restrictions with reference to the welding recovery of eroded areas. Cavitation resistant materials deposition, in hydraulic turbine runners, is an important way to reduce cavitation damage. Cobalt stainless steel is a class of steel with good cavitation resistance, mainly by their strain induced phase transformartion and lower stacking fault energy properties. The purpose of this work is to evaluate the welding metallurgy of Co Stainless Steel FCAW deposition over soft martensitic stainless steel. Cobalt stainless steel welded coatings were evaluated, as well as the influence of the heat input and gas protection in dilution, welded bead dimensions, microhardness profile and chemical composition, as well as CA6NM-HAZ microhardness and length. Preliminary results indicate a good weldability without crack and porosity in welded metal. The increase in heat input and argon+2%O_2 gas protection use promotes a dilution increase. Heat input increase and argon+2%O_2 gas protection use promote a reuction in microhardness of welded metal, mainly near fusion line, and increase in microhadness profile and length of CA6NM-HAZ. Co stainless steel coatings showed austenite and martensite phase in all tested samples. Dilution increase probably rise martensite phase content, however without hardness increase.*

Keywords: cavitation, GMAW, welding metallurgy, soft martensitic stainless steel

1. INTRODUCTION

Cavitation mass loss process occurs when a surface is exposed to a fluid with a localized pressure variation. Pressure reduction promotes the formation of bubbles, which flow to another area with increase of pressure, that collapse the gas bubbles on the surface with consequent energy release. Cavitation is frequently found in operation of hydraulic equipments as: hydropower turbine runners, valves, pumps and ships propellants (March and Hubble, 1996). Stainless steels are the most used filler materials for eroded areas. AWS ER309LSi alloy is one of the most used alloys, because of its good weldability, adequate cavitation resistance and low cost. Stainless steel alloys with cobalt commercially known as Cavitec and Cavitalloy shown better cavitation behavior compared to ER309LSi stainless steel. These alloys present low stacking-fault energy, SFE, and martensite strain induced transformation that absorb the energy of cavitation (Simoneau, 1987 and 1991).

Since the 1960s, martensitic stainless steels containing 12–13% chrome, 2–5% nickel and less than 0.06% carbon have been used to manufacture hydraulic turbines (Bilmes, et al, 2000). These steels show high yelding resistance and tenacity, high cavitation resistance and good weldability. Martensitic steels with low carbon content, such as CA6NM steel, are always quenched and tempered. The excellent tenacity of these steels occurs because of the fine dispersion of austenite on martensite during the tempering treatment at temperatures in the order of 600 ºC (Folkhard, 1988, Lippold and Kotecki, 2005). Carbon content reduction promote the formation of a soft low carbon martensite that is more resistant to hydrogen-induced cracking than standard martensitic grades (Lippold and Kotecki, 2005).

Even with good weldability and less demanding requirements with regard to pre-heating and interpass temperatures, the weld metal (WM) and the heat affected zone (HAZ) have lower impact energy and fracture tenacity than that of the base metal (BM). In general, welded structures perform less well than the base metal as the welding process results in higher levels of microstructural changes, with the formation of harder and more fragile structures (Akhtar and Brodie, 1979).

AWS ER309LSi is one of the most recommended filler metal to use with martensitic stainless steel, because their similar mechanical properties and high hydrogen-induced cracking resistance, with these filler metals low heat input can be used to minimize the thickness of the hard HAZ, (Lippold and Kotecki, 2005), however the higher cavitation resistance of the Co stainless steel, like Cavitec, can be interesting to increase the operation intervals and minimize the mass loss during cavitation.

The purpose of this work is to evaluate the welding metallurgy of Co Stainless Steel coatings on soft martensitic stainless steel with FCAW (flux cored arc welding) arc process. Heat input and gas protection influences on metal cored Cobalt Stainless Steel welded coating was evaluated, with emphasize in dilution, weld bead dimensions, microhardness and chemical composition, as well as HAZ microhardness profile.

2. EXPERIMENTAL PROCEDURES

In this work a soft martensitic stainless steel was used after 1050ºC air quenched and 580ºC tempered heat treatment, this steel was supplied by Voith Siemens company. The dimensions of the welded pieces were 75x25x25 mm. Chemical composition of the CA6NM steel and Co stainless steel 1,2mm wire are presented, Tab. 1, and FCAW parameters are visualized, Tab. 2.

FCAW coatings deposition were conduced with 150ºC interpass temperature, welding equipment used in this work was an ESAB Smashweld 315. Current and voltage were measured by Minipa ET3367 digital multimeter.

Table 1. Chemical composition of materials.

	ϕ (mm)	C (wt%)	N (wt%)	Si (wt%)	Mn (wt%)	Cr (wt%)	Ni (wt%)	Co (wt%)	Mo (wt%)	Cu (wt%)	V (wt%)	P (wt%)	S (wt%)
CA6NM		0,02	0,0	0,0	0,64	12,4	3,7	0,0	0,42	0,0	0,0	0,008	0,0018
Co wire	1,2	0,21	0,20	2,4	10,0	13,6	0,12	11,3	0,0	0,1	0,06	0,03	n/a

After visual and liquid penetrant inspection, welded samples were prepared for metallographic characterization with Buehler Isomet 4000 precision saw. Grinding and polishing were realized by Buehler Vector semi-automatic system with 220, 320, 400, 600 and 1200 mesh silicon carbide grinding paper. Metallographic polishing was realized with 3,0μm, 0,25μm monocrystalline diamond paste, and 0,04μm silica colloidal for final polishing.

Characterization was carried out by optical microscopy in an Olympus BX60 microscope, with acquisition of images through image software analysis, Analysis 5.1. Electronic microscopy was carried out by a Philips microscope model XL30 with EDX analysis. In this stage it was analyzed microstructure formation and chemical composition by EDX analysis. Mechanical property was measured by microhardness, 300gf, Vickers test in Time Microhardness equipment.

Table 2. FCAW welding parameters.

FCAW	Arc Tension (V)	Arc Current (A)	Heat Input (kJ/cm)	Welding Speed (cm/min)	Wire Speed (m/min)	Shielding gas	Shielding gas flow (l/min)	Interpasse temperature (ºC)
Cav17O$_2$	17	117	3,88					
Cav19O$_2$	19	125	4,64					
Cav22O$_2$	22	135	5,80	25	4,8	(Ar 2%O$_2$)	14	150
Cav24O$_2$	24	147	6,89					
Cav17Ar	17	117	3,88					
Cav19Ar	19	125	4,64					
Cav22Ar	22	135	5,80	25	4,8	(Ar)	14	150
Cav24Ar	24	147	6,89					

3. RESULTS AND DISCUSSION

3.1. Visual Inspection and Macrographs

Weld bead samples after liquid penetrant inspection can be visualized in Fig. 1. Heat input increase, and the use of Ar/O$_2$ for gas protection, reduce the porosity in all samples. Porosity reduction is more evident in samples that use argon for gas protection. Spatter droplets quantity increase with heat input, independently of the gas protection.
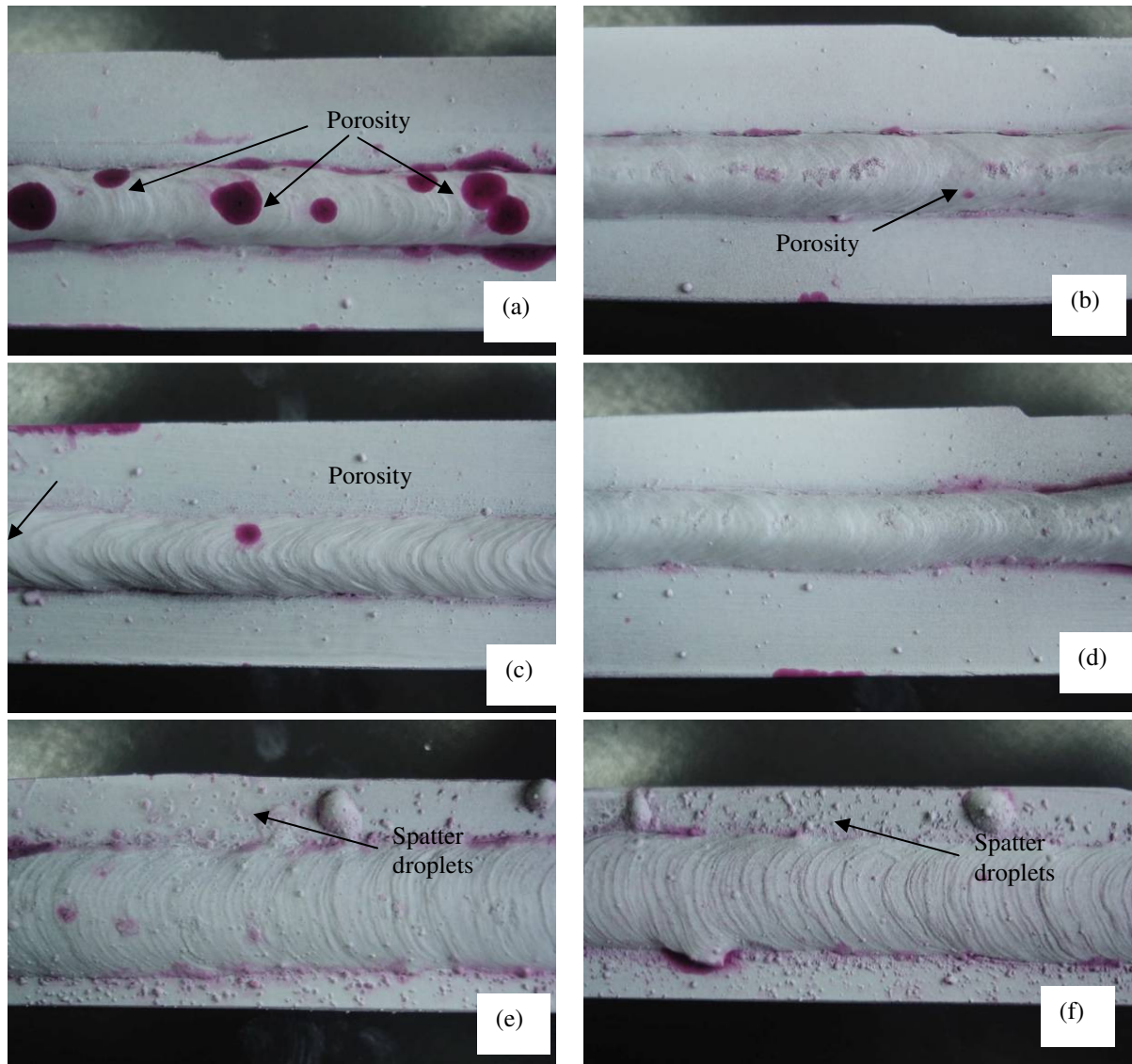
Figure 1. Weld bead after liquid penetrant liquid inspection. (a) Cav17Ar, (b) Cav17O$_2$, (c) Cav19Ar, (d) Cav19O$_2$, (e) Cav22Ar, (f) Cav22O$_2$.

Macrographs of welded samples can be observed in Fig. 2. It can be observed porosity in Cav17Ar and Cav17O$_2$, and the increase of dilution in samples with higher levels of heat input, welded with Ar and Ar/O$_2$ samples. No cracks or microcracks are observed in weld metal and CA6NM HAZ. Width/height relation, and penetration also increase with rise in heat input levels, Tab. 3. Independently of heat input used, O$_2$ adition in Ar for gas protection increase dilution and penetration in lower heat input levels, however in samples with higher levels it can observed an opposite behavior, Tab. 3.

Although dilution increases with Ar/O$_2$, width and height of welded bead did not increase, in comparison with samples that use only Ar for gas protection. Weld penetration showed a slight decrease with Ar/O$_2$ use, this probably occurs by better heat radial transfer with this gas. The better heat radial transfer can explain the penetration reduction observed in Cav22 e Cav24 samples welded with Ar/O$_2$, with better temperature distribution the weld penetration is more uniform in welded bead without deeper penetration in the center of the welded bead.

In Table 3 width/height reduction with heat input increase can be observed in Cav22 e Cav24 independently of the gas. This occurs by reduction on deposition efficiency, probably by the rise in large spatter deposits in these samples.
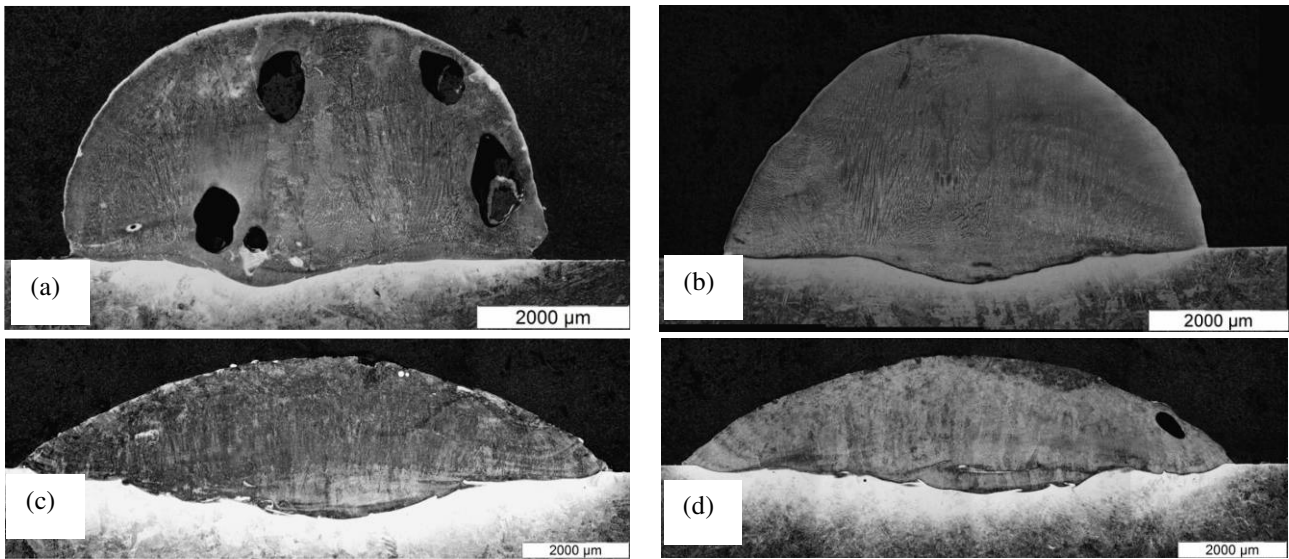
Figure 2. Cobalt stainless steel weld bead (a) Cav17Ar, (b) Cav17O$_2$, (c) Cav22Ar, (d) Cav22O$_2$.

Table 3. Weld bead dimensions and dilutions of tested samples.

FCAW	Dilution (%)	Width (mm)	Height (mm)	Penetration (mm)
Cav17Ar	3,5	7,0	3,7	0,38
Cav17O$_2$	7,5	6,8	3,4	0,43
Cav19Ar	8,4	7,3	3,6	0,50
Cav19O$_2$	11,0	7,4	3,4	0,60
Cav22Ar	24,1	11,6	2,5	0,94
Cav22O$_2$	18,0	10,4	2,2	0,83
Cav24Ar	30,8	10,5	2,2	0,85
Cav24O$_2$	38,4	9,4	1,3	0,73

3.2. Microstructure and Microhardness Evaluation

In Figure 3, welding microstructure can be observed in Cav17Ar and Cav19Ar samples. Welded microstructure showed oriented dendritic solidification. With increase in heat input and dilution, welded samples showed an increase in martensite formation, Cav22Ar, Fig. 3(f). Similar results are observed in samples welded with Ar/O$_2$ gas protection. Martensite structure formation is more clearly observed in samples with higher heat input, Fig.4(b). Otherwise dendritic solidification is more clearly observed in samples with lower heat input, and consequently lower dilution, with a probably martensite formation inside dendritic cells.

This solidification type changing can be expected in samples with more dilution because of the changing in Cr/Ni relation variation in weld metal. Even with this change in solidification mechanism, no cracks or microcracks were observed in all samples.
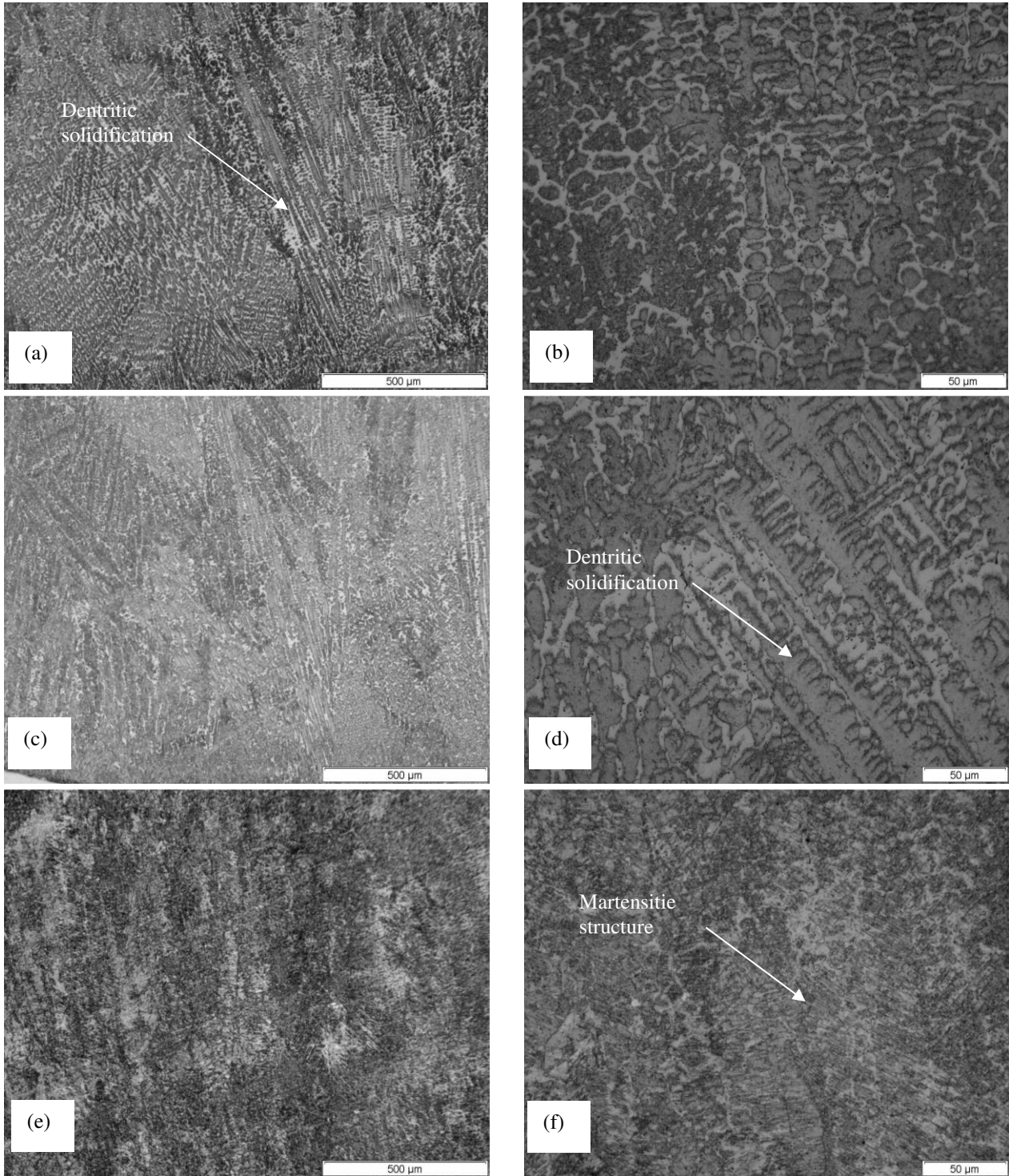
Figure 3. Cobalt stainless steel weld microstructure (a,b) Cav17Ar, (c,d) Cav19Ar, (e,f) Cav22Ar.
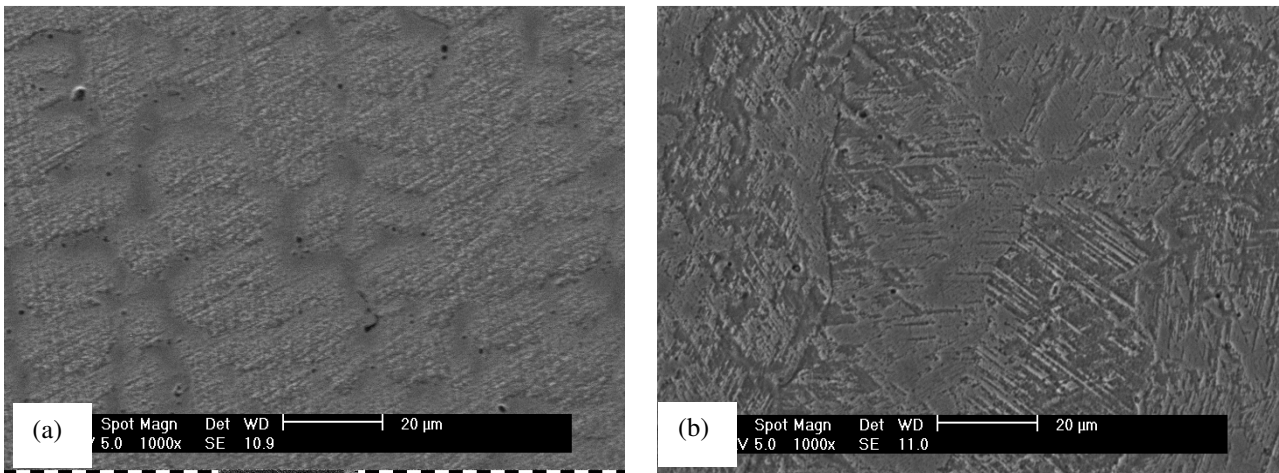
Figure 4. Cobalt stainless steel weld microstructure (a) Cav19Ar, (b) Cav22Ar.

The use of Ar/O_2 for gas protection during GMAW welding increase dilution and width/height relation in all tested samples, without modification in microstructure and solidification mechanism in Co stainless steel weldments, Fig. 3 (c,d) and Fig.5 (a,b).
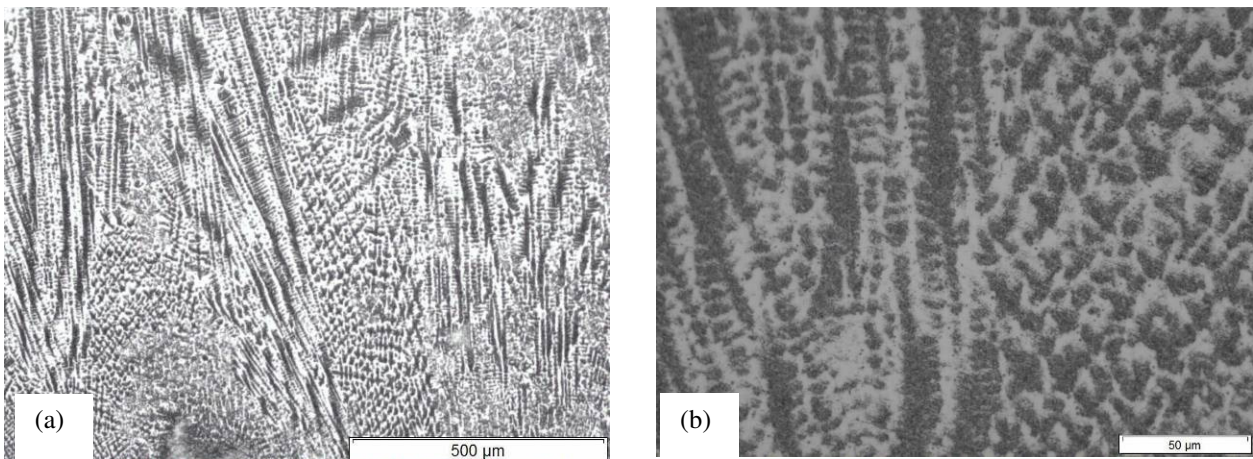

Figure 5. Cobalt stainless steel weld microstructure (a,b) Cav19O$_2$.

Chemical profile composition, evaluated by EDX, of weld metal with heat input increase can be observed in Cav19Ar and Cav22Ar, Fig. 6. It can be observed Co and Cr reduction with dilution increase, because these elements are present in major quantity in filler metal than base metal, otherwise Ni content, present only in base metal, increase with dilution, mainly near fusion line. In Figure 7 Ni increase, near fusion line, compared with samples welded without O_2 in gas protection can be observed.

Microhardness measurement profile of welded Co stainless steel showed slight difference among samples with different levels of heat input, Fig 8. It was observed a tendency to microhardness decrease in samples with higher levels of heat input, independently of the gas protection. This behavior is more clearly observed near fusion line, when samples with higher heat input showed lower microhardness values near fusion line. In this study, CA6NM HAZ microhardness and length, showed a slight increase with heat input.

These initial tests can define the better welding parameters, with intend to obtain lower levels of porosity and good bead dimensions, with lower levels of dilution and penetration. The parameter that obtain these requirements was Cav22O$_2$, because their good stability, lower levels of porosity without excessive dilution and spatter droplets formation.
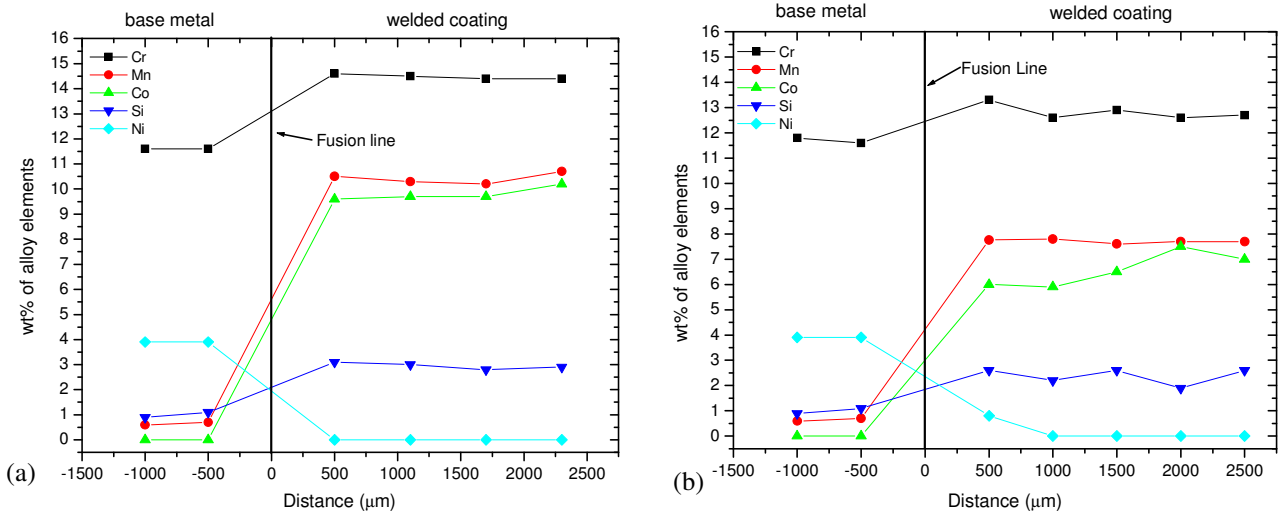
Figure 7. Cobalt stainless steel chemical composition profile (a) Cav19Ar, (b) Cav22Ar.
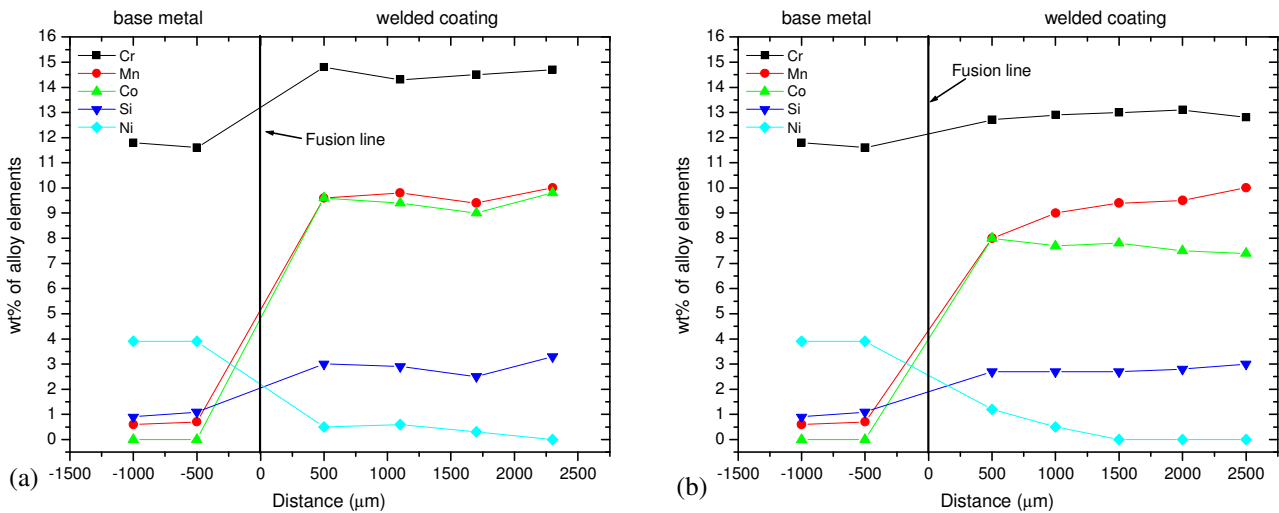

Figure 8. Cobalt stainless steel chemical composition profile (a) Cav19O$_2$, (b) Cav22O$_2$.
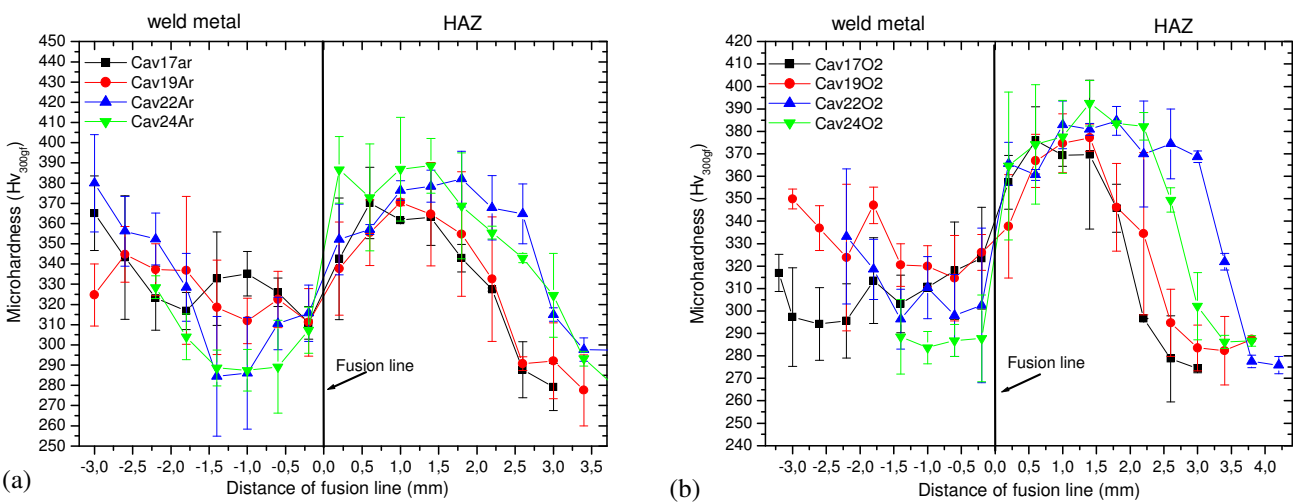

Figure 9. Cobalt stainless steel microhardness profile (a) Ar gas protection, (b) Ar/O$_2$ gas protection.

4. CONCLUSIONS

The increase in heat input promotes a dilution increase as well as width/height relation. HAZ microhardness and length showed a slight increase with heat input. Porosity and superficial defects reduction were observed with heat input increase, otherwise large spatter deposits and decrease in deposition efficiency were observed in samples with higher levels of heat input. Argon+2%O_2 gas protection promote a dilution increase and reduce porosity in samples with lower heat input.

Co stainless steel welded coatings showed austenite and martensite phase with increase in martensite with base metal dilution increase.

These initial tests are very important to define the better welding parameters to obtain lower levels of porosity and good bead dimensions in association with lower levels of dilution and penetration. The parameter that obtain these requirements was Cav22O_2, because their good stability, lower levels of porosity without excessive dilution and better deposition efficience.

5. ACKNOWLEDGMENTS

The authors thank the financial support of the CNPq, Institute of Technology for Development, LACTEC for the wires used in this work and Voight for the CA6NM used in this work.

6. REFERENCES

Akhtar A and Brodie N W, 1979, "Field-Welding Large Turbine Runners", Water Power & Dam Construction, pp. 40–46.

Bilmes P.D., Llorente, C., Ipiña, J.P., 2000, "Toughness and Microstructure of 13Cr4NiMo High-Strength Steel Welds", Journal of Materials Engineering and Performance, Vol. 9, No. 6, pp. 609–615.

Folkhard E,, 1988, "Welding Metallurgy of Sainless Steels". Springer- Verlag, New York, 279 p.

Lippold, J.C. and Kotecki, D., 2005, "Welding metallurgy and weldability of stainless steel", John Wiley & Sons, New Jersey, 2005, 357p.

March, Patrick, and Hubble, Jerry, 1996, "Evaluation of Relative Cavitation Erosion Rates For Base Materials", Weld Overlays, and Coatings. Report No. WR28-1-900-282, Tennessee Valley Authority Engineering Laboratory. Norris, TN.

Simoneau, R.L.P., 1987, "Cavitation Erosion and Deformation Mechanism of Ni and Co Austenitic Stainless Steel", Proceedings of 7th Conference on Erosion by Liquid and Solid Impact, Cambridge, Inglaterra.

Simoneau, R.L.P., 1991, "Jet and Hydro turbine Cavitation Erosion", Cavitation and Multiphase Flow Forum, American Society of Mechanical Engineers.

5. RESPONSIBILITY NOTICE

The authors are the only responsible for the printed material included in this paper.